



Influence of Sm and Nb on the structural, electric, magnetic and magneto-electric properties of BaTiO₃-Li_{0.5}Fe_{2.5}O₄ composite ceramics grown by the conventional solid state technique

Ganapathi Rao Gajula¹ · Lakshmi Rekha Buddiga² · K. N. Chidambara Kumar¹ · Madhavaprasad Dasari³

Received: 6 October 2018 / Accepted: 15 November 2018 / Published online: 17 November 2018
© Springer Science+Business Media, LLC, part of Springer Nature 2018

Abstract

The Sm and Nb doped BaTiO₃-Li_{0.5}Fe_{2.5}O₄ composite ceramics having chemical formulae (90)BaTi_(1-2x)Nb_xSm_xO₃ + (10) Li_{0.5}Fe_{2.5}O₄ ($x = 0, 0.05$ and 0.1) were synthesized using conventional solid state technique. The structural, morphological, magnetic, dielectric, ferroelectric and magneto-electric properties of composites have been studied. The XRD measurement reveals the absence of peaks pertaining to impurities and strongly confirms the high crystalline nature of all the composites. From FESEM images, the average grain size of composites increases with increase in the concentration of Nb and Sm. The VSM studies confirm the soft magnetic nature of all the composites. The dielectric measurements confirm the increase in the transition temperature (T_c) of the BTL composite with an increase in the concentration of Nb and Sm. The P–E studies confirm that the ferroelectric nature of the BTL composite softens after doping Nb and Sm in it. The ME voltage coefficient value confirms the uniform growth of grains in all the composites and reveals a strong interaction between ferroelectric and magnetic orders.

1 Introduction

The research on the multiferroic materials have increased enormously because of the coupling between electric phase and magnetic phase. The multiferroic materials have received more attraction in the field of research on account of their advanced fundamental nature and technological importance. Multiferroic material combines any two or more of the ferroic order such as ferroelectric, ferromagnetic, ferroelastic, ferrotoroidic, ferroelasticity, ferroelectricity, anti-ferromagnetism and ferrimagnetism. The multiferroic materials exhibit ferroelectric nature and ferromagnetic nature simultaneously and have a wide range of potential applications in the fields like magnetoelectric sensors, magneto capacitive devices, information storage, electrically driven

magnetic data storage, spintronics, electro-optic devices and recording [1–3]. Magnetoelectric (ME) effect is an induced dielectric polarization by an external magnetic field or an induced magnetization by an external electric field [4]. This ME effect occurs in the multiferroic composites and it is absent in an individual constituent phases [5, 6]. It is highly desirable to combine ferroelectric and ferromagnetic order within one material.

The BaTiO₃ (BT) is one among the good ferroelectric material possessing perovskite structure ABO₃. It is an often used material possessing dielectric nature, piezoelectric nature and ferroelectric nature. The applications of BT material include its use in capacitors, thermistors, electro-optic devices and in the electronics industry. The Li_{0.5}Fe_{2.5}O₄ (LF) is a spinel-type soft ferrite which possesses high saturation magnetization, high Curie temperature and square-loop properties. Rare-earth oxides are known to be useful dopants for ceramic dielectrics due to their functions of stabilizing the temperature dependence of dielectric constant and lowering the dissipation factor. Extensive works on rare-earth ion doped in the BT-based dielectrics have been carried out, such as crystal defect chemistry of rare earth cations in BT [7]. Substitution of lanthanides in barium titanate is of great significance in the modern electronic industry. So, rare earth metals like samarium (in varying concentrations)

✉ Ganapathi Rao Gajula
ganapathi.gajula@gmail.com

¹ Department of Physics, BS&H, Sree Vidyanikethan Engineering College, Tirupati, A.P 517102, India

² Department of Chemistry, Andhra University, Visakhapatnam, A.P 530 003, India

³ Department of Physics, GIT, GITAM University (deemed to be university), Visakhapatnam, A.P 530 045, India

have been doped in barium titanate material [8–10]. The microstructure, dielectric and ferroelectric properties of BT can be modified by a wide variety of substitutions possible at Ba^{2+} on A sites or Ti^{4+} on B sites independently or simultaneously in perovskite structure. These substitutions can be isovalent or heterovalent. The effects of isovalent substitutions such as Pb^{2+} , Ca^{2+} , Sr^{2+} for Ba^{2+} on A sites and Zr^{4+} , Hf^{4+} , Mn^{4+} for Ti^{4+} on B sites on microstructure, dielectric properties of BT ceramics have been investigated [11–16]. The heterovalent substitutions such as Mg^{2+} , Dy^{3+} , Tb^{3+} , Eu^{3+} , Nd^{3+} , Gd^{3+} , Yb^{3+} , Sm^{3+} , Er^{3+} , Ho^{3+} , Sb^{3+} , Sc^{3+} , La^{3+} , Nb^{5+} , Bi^{3+} and so forth for Ba^{2+} or Ti^{4+} cause charge imbalance and creation of vacancies on A sites or B sites or generation of holes to maintain electrical charge neutrality [17–25]. The rare earth dopants are one of the most important substitutions. BaTiO_3 doped with lanthanides have been explained to exhibit electron paramagnetic resonance [26].

Addition of samarium can restrain the grain growth of barium titanate ceramics and lead to the fall of the Curie temperature. There is diffuse phase transition in Nb and Sm doped barium titanate ceramics. Sm^{3+} ions can decrease the dielectric loss of barium titanate ceramics on the basis of the Ti-vacancy defect compensation model. The remnant polarization and the coercive field of Nb and Sm-doped barium titanate ceramics either decrease or increase based on the difference of ionic radius of elements. As temperature rises, the remnant polarization and the coercive electric field of Sm-doped barium titanate ceramics decrease simultaneously [11]. The dielectric properties of BaTiO_3 can be modified by the addition of the dopants such as La^{3+} , Mn^{4+} , Nb^{5+} , and Zr^{4+} to occupy Ba^{2+} on A sites or Ti^{4+} on B sites to form the solid solution [17, 27, 28].

Based on the above discussion, we present here the structural, electric and magnetic properties of Sm and Nb doped $\text{BaTiO}_3\text{-Li}_{0.5}\text{Fe}_{2.5}\text{O}_4$ composite ceramics in this paper. The composites having chemical formulae $(90)\text{BaTi}_{1-(2x)}\text{Nb}_x\text{Sm}_x\text{O}_3 + (10)\text{Li}_{0.5}\text{Fe}_{2.5}\text{O}_4$ ($x=0, 0.05$ and 0.1) are represented as $(90)\text{BaTiO}_3 + (10)\text{Li}_{0.5}\text{Fe}_{2.5}\text{O}_4$ (BTL), $(90)\text{BaTi}_{0.9}\text{Nb}_{0.05}\text{Sm}_{0.05}\text{O}_3 + (10)\text{Li}_{0.5}\text{Fe}_{2.5}\text{O}_4$ (BTNS1) and $(90)\text{BaTi}_{0.8}\text{Nb}_{0.1}\text{Sm}_{0.1}\text{O}_3 + (10)\text{Li}_{0.5}\text{Fe}_{2.5}\text{O}_4$ (BTNS2).

2 Experimental method

The $(90)\text{BaTi}_{1-(2x)}\text{Nb}_x\text{Sm}_x\text{O}_3 + (10)\text{Li}_{0.5}\text{Fe}_{2.5}\text{O}_4$ ($x=0, 0.05$ and 0.1) composites ceramics were synthesized using conventional solid state technique. The analytical purity of compounds were BaCO_3 (98%) (Merck), TiO_2 (99.5%), Li_2CO_3 (99%), Fe_2O_3 (98%) (Loba Chemie), Nb_2O_5 (99.9%) (Titan biotech Ltd.), Sm_2O_3 (99.9%) (Loba Chemie). All the materials were weighed accurately in the required stoichiometric ratio and mixed together in an agate mortar. The grinding process is carried out for 10 h to obtain a homogeneous

mixing and distribution of the ingredients. These samples were calcinated at 900°C temperature for 3 h. The calcination process involves heating, as a result of which the homogeneous mixer of starting materials decomposes. The calcinated powder is grinded for 3 h to achieve a fine powder so as to reduce the particle size and promote fine mixing of any residual unreacted oxide.

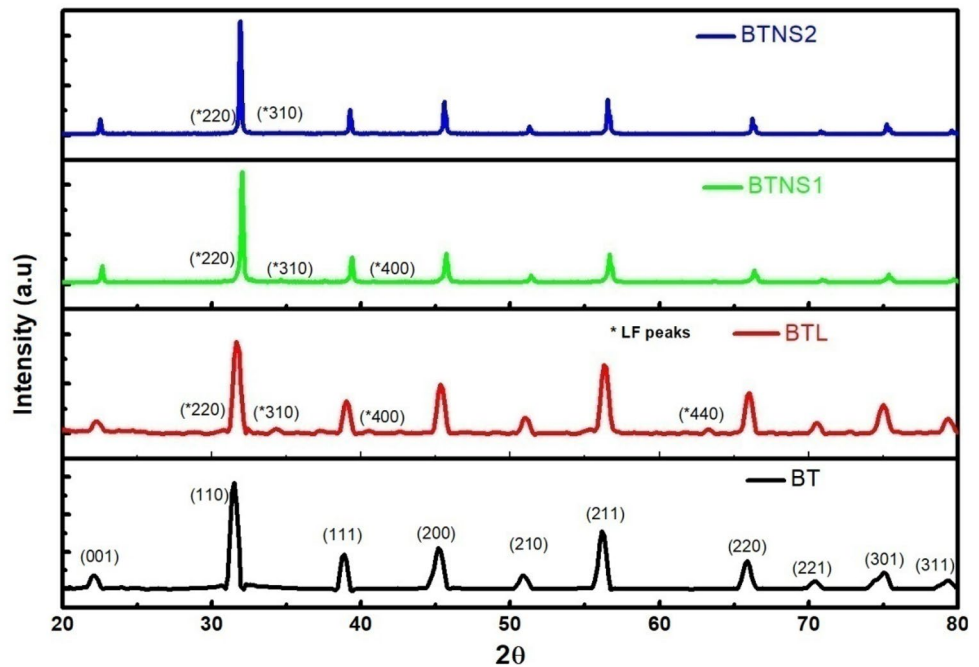
A saturated solution of PVA called a binder is mixed with the calcinated powder and grinded in order to obtain homogeneous material. The powder is then shaped into pellets by using hydraulic press. In order to prepare pellets, a die set is used. The powder is placed in the die set and pressed by applying pressure using hydraulic press. All the samples of pellets are sintered at temperature 1150°C for 3 h. Sintering involves large scale diffusion, resulting in the formation of the final product which can analysed for its structural, magnetic, dielectric and ferroelectric properties using different techniques. The structural and morphological studies were carried out using Bruker D8 Advance X-ray diffractometer and Carlzeiss ultra-55 FESEM/EDAX. The magnetic, dielectric and ferroelectric measurements were carried out using vibrating sample magnetometer (Quantum Design PPMS, Model 6000), broadband dielectric spectrometer (Wayne Kerr Electronics Pvt. Ltd., Model: 1J43100) and P–E loop tracer (TF analyzer 2000) respectively. The magneto-electric voltage coefficient (α_{ME}) was measured with respect to the DC magnetic field (H_{dc}) by superimposing 1 Oe AC magnetic field generated by Helmholtz coils at a frequency of 1 kHz using SR 830 DSP lock-in amplifier.

3 Results and discussions

3.1 X-ray diffraction

The X-ray diffraction patterns of sintered ceramics BT, BTL, BTNS1 and BTNS2 recorded at room temperature are shown in Fig. 1. The diffraction peaks of pure BT and all composites are well indexed using JCPDS cards no 79-2263. The X-ray diffraction pattern of BT reveals the formation of single phase tetragonal perovskite structure. The XRD peaks at 2θ values 30.56° , 34.34° , 40.34° and 63.29° indexed as (220), (310), (400) and (440) respectively represents the presence of LF (indicated as * in Fig. 1) in the grown composites. The diffraction peaks of all the composites reveal the formation of the tetragonal perovskite structure with small ferrite phase. We have indexed the diffraction peaks of LF in composites BTL, BTNS1 and BTNS2 using JCPDS no. 89-7832 & 88-06711. The absence of extra peaks pertaining to impurities strongly confirms the high crystalline nature of all the composites. The composites show both the ferroelectric phase and low ferrite without any structural change in its constituent phases [29]. The diffraction peaks

Fig. 1 X-ray diffraction pattern of BT, BTL, BTNS1 and BTNS2



of BTNS1 and BTNS2 have shifted towards higher diffraction angle and this strongly confirms the incorporation of Nb and Sm in BTL.

The lattice parameters of ferroelectric phase have been calculated from the relation

$$d_{hkl} = \frac{1}{\sqrt{\frac{h^2+k^2}{a^2} + \frac{l^2}{c^2}}} \quad (1)$$

The lattice parameters of ferrite phase have been calculated from the relation

$$d_{hkl} = \frac{a}{\sqrt{h^2 + k^2 + l^2}} \quad (2)$$

The values of lattice parameters for ferroelectric and ferrite phase of all the samples are tabulated in Table 1. We see from Table 1, the lattice parameters for the two phases in composites are almost equal to its constituent phases. This representing that no structural changes have occurred

with varying Nb and Sm elements in place of Ti [30]. These results can be explained by the substitution model, where Li^{1+} ions substitute for Ba^{2+} at A-site and Fe^{3+} ions substitute for Ti^{4+} , co-doping of Nb and Sm at B-site [31].

The amount of constituent phases approximately present in BT, BTL, BTNS1 and BTNS2 ceramics after sintering is calculated using the corresponding intensity peaks [32] which is presented in Table 1. The percentage of phases is calculated by the relation

$$\% \text{ of phases} = \frac{I_{\text{ferroelectric/ferrite}}}{I_{\text{ferroelectric}} + I_{\text{ferrite}} + I_{\text{unknown}}} \times 100 \quad (3)$$

The average crystallite size of composite materials is calculated using Debye Scherrer's relation

$$D = \frac{k\lambda}{\beta_1 \cos \theta} \quad (4)$$

where k is the shape factor = 0.94, β_1 is the full width at half maximum (FWHM) in radians, λ is the wavelength of the

Table 1 Lattice parameters, constituent phases and average crystallite size of the BT, BTL, BTNS1 and BTNS2 composite ceramics

Composition (x)	Lattice parameters of phase (Å)				Phase percentage		Average crystallite size (nm)	
	Ferrite a	Ferroelectric			Ferrite	Ferroelectric	Ferrite	Ferroelectric
		a	c	c/a				
BT	–	4.010	4.012	1.005	–	100	–	15.97
BTL	8.504	4.002	4.007	1.001	0.343	99.65	14	15.94
BTNS1	8.231	3.980	3.963	0.995	2.568	97.43	75.94	61.98
BTNS2	8.217	3.986	3.975	0.997	1.068	98.61	78.56	45.21

X ray source of radiation whose value is 1.5406 \AA and θ is the Bragg's diffraction angle. The average crystallite size of the grown composites is shown in Table 1. The average crystallite size of the ferrite increases with substitution of Nb and Sm in BTL and slightly increases with an increase Nb and Sm in BTNS1. We see from Table 1 that the crystallite size of BTL composite increases as Nb and Sm are doped in the BTL which clearly indicates the enhancement in the crystalline nature of the composite. This is also evident from the XRD spectrum shown in Fig. 1.

3.2 Morphological studies

The FESEM micrographs of BT, BTL, BTNS1 and BTNS2 are shown in Fig. 2. We see from Fig. 2, particle distribution gives non homogenous morphology to micro sized grains. We observe non homogenous grains of various sizes in all the samples. The FESEM micrographs confirm the coarseness in the samples with low porosity. All the samples exhibit dense micro structure with clear grain boundaries.

The dense microstructure gives the enhancement of electrical properties of composites [31]. The larger grains are formed due to an agglomeration or chemical reaction or inter diffusion taking place between the two phases. The grain morphology of the BTNS1 and BTNS2 is changed due to Nb and Sm substituted in BTL. The shape of the grains of BT, BTL seems to be spherical, BTNS1 seems to be cylindrical and BTNS2 seems to be surface of the custard apple. The average grain sizes of all the samples are calculated using imageJ software shown in Table 2. We see from Table 2, the

Table 2 The average grain size of BT, BTL, BTNS1 and BTNS2 ceramics

Sample	Average grain size (μm)
BT	1.363
BTL	1.163
BTNS1	1.164
BTNS2	1.774

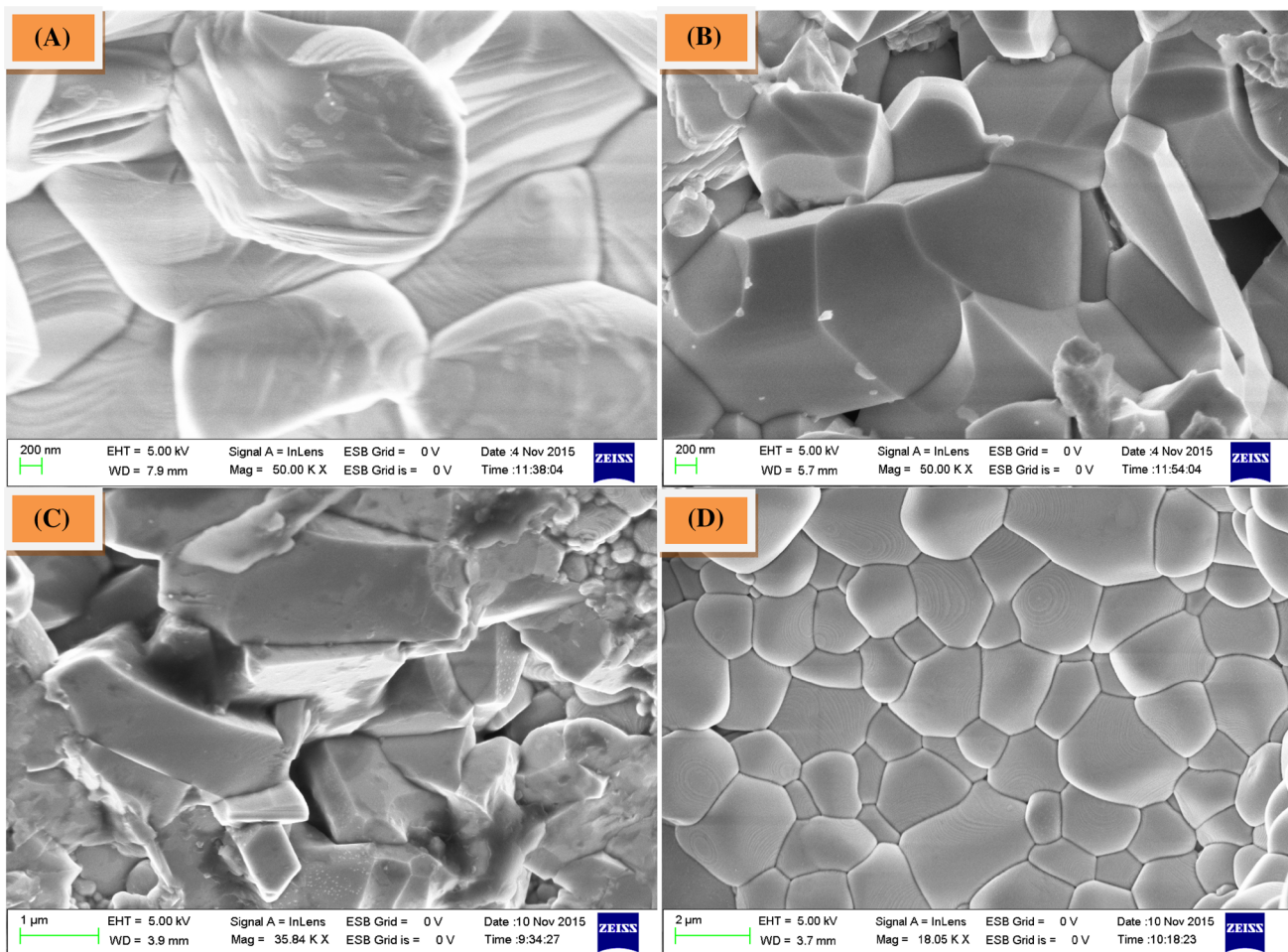


Fig. 2 FESEM micrographs of the BT, BTL, BTNS1 and BTNS2 composite ceramics

average grain size of composites increases with increase in the concentration of Nb and Sm in BTL.

The energy dispersive X-ray spectra (EDAX) of all the samples are shown in Fig. 3. We see from Fig. 3, all the samples exhibits elements which are proportional to stoichiometric ratio of powders used in synthesis of samples. From Fig. 3, we also see that no other elements other than Ba, Ti, O, Fe, Nb and Sm are observed in all composites of spectra. Hence impurities are not present in the composites which strongly confirm the high crystalline nature of all the samples and this is also evident from the XRD spectrum shown in Fig. 1. But Li element is not recorded in all composites due to low atomic number.

3.3 Ferroelectric properties

The variation of the polarization with an electric field (P–E loops) observed at room temperature for samples BTL, BTNS1 and BTNS2 are shown in the Fig. 4. We observe from Fig. 4, that all the composites have no proper

saturation polarization which clearly indicates the existence of a leakage current [33]. The leakage current of BTL composite is decreases upon doping it with Sm and Nb. The saturation polarization, remnant polarisation and coercive field of BTL, BTNS1 and BTNS2 are depicted in Table 3. The saturation polarisation and remnant polarisation of BTL are high in comparison with all the composites and both the saturation polarisation and the remnant polarisation decrease with the substitution of Nb and Sm in BTL. The coercive field of BTL composite is high in comparison with all the composites. Upon doping Sm and Nb in BTL, the coercive field decreases initially and again increases when the concentration of Sm and Nb is increased in BTL. This might be due to the effect of an oxygen vacancy and the grain size [34]. Hence the addition of Nb and Sm in BTL softens BTL composite because the saturation polarisation, remnant polarisation and the coercive field of BTL composite decreases upon adding Nb and Sm in BTL composite [35].

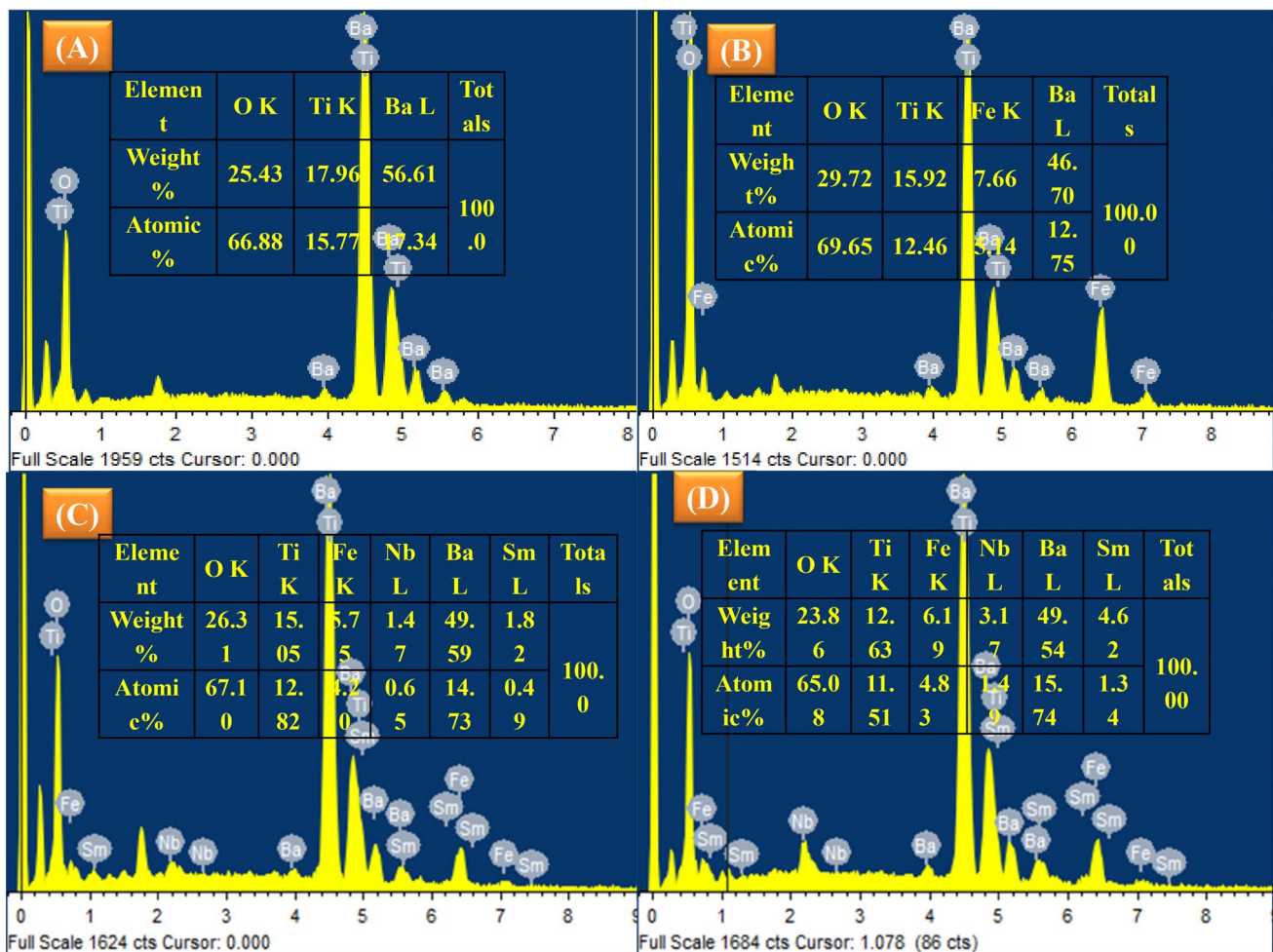


Fig. 3 EDAX spectrum of the BT, BTL, BTNS1 and BTNS2 composite ceramics

Fig. 4 Ferroelectric properties of BTL, BTNS1 and BTNS2 composite ceramics. Inset shows larger view of the BTNS1 and BTNS2

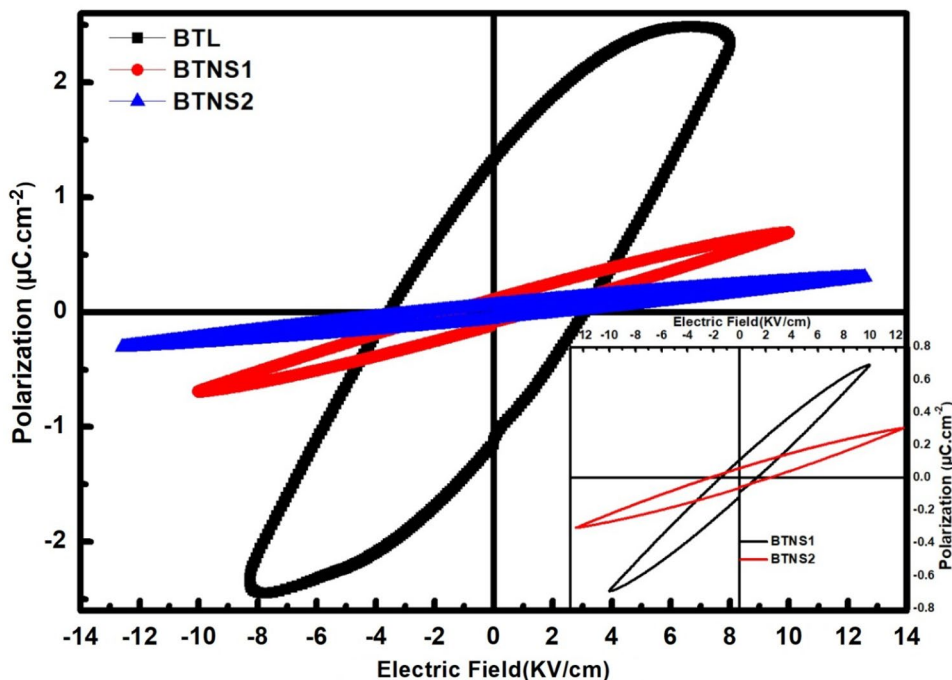


Table 3 The values of saturation polarization, remnant polarization and coercive field

Sample	Saturation polarization (P_s) $\mu\text{C}/\text{cm}^2$	Remnant polarization (P_r) $\mu\text{C}/\text{cm}^2$	Coercive field (E_c) kv/cm
BTL	2.39	1.32	3.55
BTNS1	0.69	0.108	1.485
BTNS2	0.31	0.058	2.29

3.4 Dielectric studies

3.4.1 Dielectric constant (ϵ') varies with temperature

The variation of dielectric constant (ϵ') of BTL, BTNS1 and BTNS2 composites with temperature at frequencies 1 kHz, 10 kHz, 100 kHz and 1 MHz are shown in Fig. 5. From Fig. 5, we clearly see that the dielectric constant of BTL decreases with increase in temperature upto a certain temperature at all frequencies and beyond this certain temperature, the dielectric constant increases steeply and becomes maximum at a temperature called transition temperature. At transition temperature, a transformation from ferroelectric to paraelectric takes place and this transition temperature is also referred as Curie temperature. Beyond this temperature the dielectric constant decreases with increase in temperature. The dielectric constant of BTL decreases initially with increase in temperature upto 183 °C, 230 °C, 290 °C and 402 °C at frequencies 1 kHz, 10 kHz, 100 kHz and 1 MHz respectively and beyond these temperatures, the dielectric

constant increases and reaches maximum at temperatures 383 °C, 452 °C, 523 °C and 588 °C for frequencies 1 kHz, 10 kHz, 100 kHz and 1 MHz respectively. The transition temperatures of BTL at frequencies 1 kHz, 10 kHz, 100 kHz and 1 MHz are 383 °C, 452 °C, 523 °C, and 588 °C respectively. The peak at transition temperature is sharp for frequency 1 kHz and this peak broadens out at frequencies 10 kHz and 100 kHz. A kink is observed at temperature 588 °C for frequency 1 MHz. The value of dielectric constant of BTL is higher at 1 kHz which is 2145. The value of dielectric constant of BTL decreases with increase frequency and transition temperature of BTL increases with increase in frequencies.

The nature of the dielectric constant of BTNS1 is same as that of the BTL composite. The dielectric constant of BTNS1 decreases initially with increase in temperature up to 147 °C, 200 °C, 257 °C and 333 °C at frequencies 1 kHz, 10 kHz, 100 kHz and 1 MHz respectively. Beyond those temperatures, the dielectric constant increase with increases in temperature and the dielectric constant becomes maximum at a temperature called transition temperature. The transition temperatures of BTNS1 at frequencies 1 kHz, 10 kHz, 100 kHz and 1 MHz are 333 °C, 420 °C, 518 °C and 596 °C respectively. At 1 MHz, the dielectric constant of BTNS1 becomes more broadening. The transition temperature of BTNS1 is lower than the transition temperature of BTL for frequencies 1 kHz, 10 kHz and 100 kHz and the dielectric constant of BTNS1 is lower than BTL at frequencies 1 kHz, 10 kHz, 100 kHz, 1 MHz due to substitution of Nb, Sm in BTL.

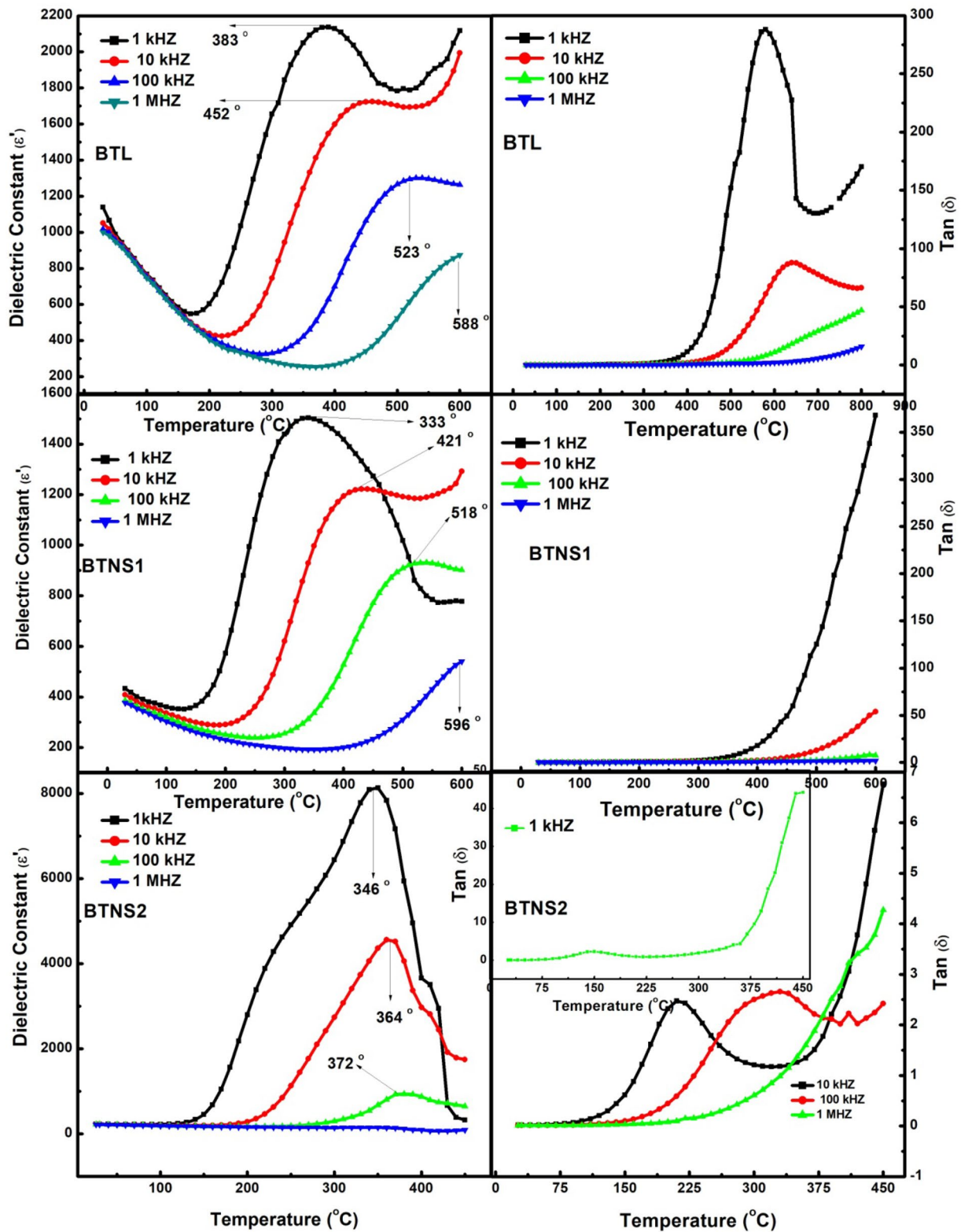


Fig. 5 Variation of dielectric constant (ϵ') and dielectric loss ($\tan \delta$) of BTL, BTNS1 and BTNS2 composite ceramics with temperature at 1 kHz, 10 kHz, 100 kHz and 1 MHz

The dielectric constant of BTNS2 is almost constant initially with increase in temperature upto 119 °C, 149 °C and 229 °C at frequencies 1 kHz, 10 kHz and 100 kHz respectively. Beyond those temperatures, the dielectric constant increases with increases in temperature and the dielectric constant becomes maximum at a temperature called transition temperature. At 1 MHz, the dielectric constant of BTNS2 is almost constant at all the temperatures. The transition temperatures of BTNS2 at frequencies 1 kHz, 10 kHz and 100 kHz are 346 °C, 364 °C and 372 °C respectively. Beyond these temperatures, the dielectric constant of BTNS2 decreases steeply with increase in temperature. The sharp transition peaks of BTNS2 are shifted towards higher temperature with increase in frequencies. The dielectric constant of BTNS2 is greater than BTNS1 and BTL. The transition temperature of BTNS2 at 1 kHz is greater than BTNS1 and is less than BTL. At frequencies 10 kHz and 100 kHz, the transition temperature (T_c) of BTNS2 is less than BTNS1 and BTL which may be due to grain size [36]. The transition temperature (T_c) decreases with increasing grain size which is obtained in FESEM studies shown Table 2.

The maximum value of the dielectric constant at lower frequencies is due to the space charge polarization effect at the interface between BT and LF phases [37–39]. And also due to electron hopping mechanism between Fe^{3+} and Fe^{2+} by applying external electric field then dipoles between $Fe^{3+} \leftrightarrow Fe^{2+}$ orient their axes parallel to the applied field [40, 41]. The decreasing value of the dielectric constant of all the samples with increase in the temperature is due to random vibration motion of electrons [41, 42]. The value T_c is frequency dependent and increases with frequency as the diffuse phase transition and frequency dispersion characteristics suggest relaxor behaviour of the prepared solid solution of composites [43]. The phase transition peaks of the composites become gradually broadened. This suggests that the partial substitution of Nb^{5+} and Sm^{3+} for Ti^{4+} induces a diffusive phase transition in the ceramics with high level of Li^{1+} , it may lead to the increment in the disorder degree of B-site ions and the local compositional variations [44].

3.4.2 Dielectric loss ($\tan \delta$) varies with temperature

The variation of the dielectric loss ($\tan \delta$) of BTL, BTNS1 and BTNS2 composites with temperature at frequencies 1 kHz, 10 kHz, 100 kHz and 1 MHz are shown in Fig. 5. We see from Fig. 5, the dielectric loss of all composites almost constant initially with increase in temperature upto certain temperature. The dielectric loss of BTL follows trends same as dielectric constant of BTL. At frequency 1 kHz, beyond the temperature 400 °C, the dielectric loss of BTL increases steeply with increase in temperature upto 590 °C then decreases steeply with increase in temperature. The dielectric loss of BTL is decreases with increase

in high temperature region. The dielectric loss of BTNS1 is increases steeply with increase in temperature beyond 370 °C, 466 °C at frequency 1 kHz, 10 kHz respectively. The dielectric loss BTNS1 is almost constant at high frequencies. The dielectric loss of BTNS2 exhibits small kink at 147 °C at frequency 1 kHz, beyond the temperature 368 °C, the dielectric loss of BTNS2 increases steeply with increase in temperature which shown in set of Fig. 5. At frequency 10 kHz, beyond the temperature 110 °C, the dielectric loss of BTNS2 increases steeply with increase in temperature upto 210 °C then dielectric loss of BTNS2 is decreases with increase in temperature. At frequency 100 kHz, beyond the temperature 165 °C, the dielectric loss of BTNS2 increases steeply with increase in temperature upto 326 °C then dielectric loss of BTNS2 is decreases with increase in temperature. At frequency 100 MHz, the dielectric loss of BTNS2 increases steeply with increase in temperature beyond 204 °C. The dielectric loss of composites is decrease with increase in concentration of Nb and Sm in BTL at all frequencies might be due to substitution of Nb^{5+} and Sm^{3+} for Ti^{4+} with LF. As frequency increases, the dielectric loss decreases with increasing temperature. Below the peak temperature, $\tan \delta$ increases due to the hopping rates of electrons between $Fe^{+3} \leftrightarrow Fe^{+2}$ increases with increasing temperature. At the peak value, the frequency of hopping is equal to the frequency of AC field. The maximum dielectric loss can be explained by Koop's model, this peak obtained from grain boundaries contains impurities [45].

3.5 Magnetic properties

3.5.1 M–H curve

The M–H loop of all the composites measured at room temperature (300 K) is shown in Fig. 6. The inset shown in Fig. 6 strongly confirms the presence of low ferromagnetic ordering in the composites. The variation of saturation magnetisation (M_s), remnant magnetisation (M_r) and coercive field (H_c) of BTL composite with the various concentrations of Nb and Sm are shown in Fig. 7. The values of saturation magnetization (M_s), remnant magnetization (M_r) and coercive magnetic field (H_c) for all the composites are shown Table 4. We see from Table 4, the saturation magnetization and remnant magnetization of composites decreases with increase in the concentration of Nb and Sm in BTL (clearly shown in Fig. 7). The decrease in the value of saturation magnetization (M_s) is attributed to the formation of antiphase boundaries in composites [46]. The reason for the decrease in the remnant magnetization of BTL composite with increase in the concentration of Nb and Sm might be due to the replacement of few Ti ions with Nb and Sm ions, as a result of which the magnetic interactions between the ferrite grains

Fig. 6 Magnetization of the BTL, BTNS1 and BTNS2 composite ceramics varies with the magnetic field. Inset shows magnified view of magnetization curves at low applied magnetic field

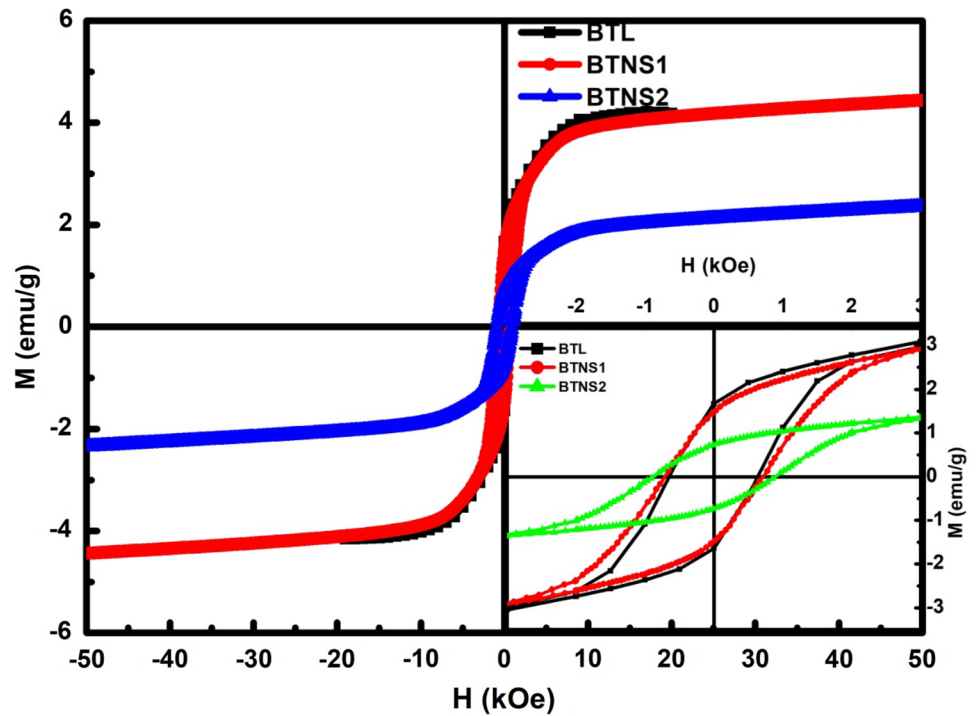
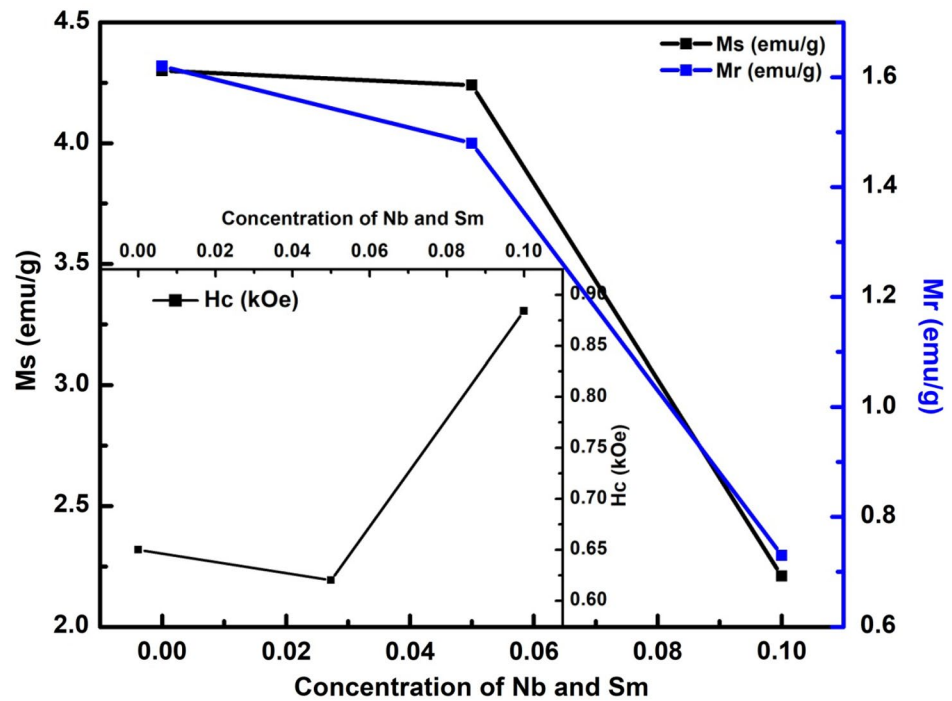


Fig. 7 Saturation magnetization (M_s), remnant magnetization (M_r) and Coercive field varies with concentration of Nb and Sm



reduces. As the super exchange interaction is sensitive to bond angles and bond distances, the spiral spin structure might be destroyed completely by co-doping of Nb and Sm in place of Ti^{4+} in BTL which leads to the release of latent magnetization and the changes of remnant magnetization in composites [47]. The coercive field (H_c) of composites

strongly depends on the grain size and morphology. The coercive field of the BTL composites are decreases by a small amount initially with the substitution of Nb and Sm in BTL and later increases drastically with an increase in the concentration of Nb and Sm, which might be due to the change in the grain size of the composites. Any material

Table 4 The values of saturation magnetization (M_s), remnant magnetization (M_r), coercive magnetic field (H_c), squareness and magnetic moment (μ_B) of BTL, BTNS1 and BTNS2 composite ceramics

Sample	Ferro magnetic parameters			Square-ness	Magnetic moment (μ_B)
	M_s (emu/g)	M_r (emu/g)	H_c (kOe)		
BTL	4.30	1.62	0.65	0.3767	0.1775
BTNS1	4.24	1.48	0.62	0.3490	0.1800
BTNS2	2.21	0.73	0.884	0.3303	0.0964

which has low coercivity exhibit soft magnetic nature and hence since all the composites have very low coercivity value (shown in Table 4), we strongly confirm the soft magnetic nature of all the composites.

The larger grain contains more domains with Bloch walls which can move more easily under an applied field than the reversal of magnetization required in single domain particles. Thus H_c changes with a change in the grain size [48] (shown in Table 2).

The magnetic moment of the composites in terms of Bohr magneton is calculated using the following relation [49]

$$\mu_B = \frac{M_s x M}{5585} \quad (5)$$

where μ_B is Bohr's magneton, M_s is saturation magnetization, M is the molecular weight and 5585 is the magnetic factor and shown in Table 4.

The magnetic moment of composites initially increases by a small amount and later decreases with further increase

in the concentration of Nb and Sm. The change in values of the magnetic moment (μ_B) may be a contribution of the Nb and Sm grains which act as centers of magnetization [50].

The squareness of the composites is calculated using the ratio (M_r/M_s) and shown in Table 4. The squareness value of all the composites are low and almost remains constant with an increase in concentration of Nb, Sm which also confirms the soft magnetic nature of all the composites.

3.5.2 M–T curve

Figure 8 shows the variation of the magnetization of all the composites with temperature. We see from Fig. 8, the magnetization of all the composites increase by a small value with an increase in the temperature upto certain temperature called transition temperature (T_c). At the transition temperature, the composites change from ferromagnetic phase to paramagnetic phase. Beyond the transition temperature, the magnetization of all the composites decreases suddenly to nearly zero value. The temperature at which the magnetization becomes zero is called Neel temperature (T_N). The transition temperature and neel temperature of all the composites are shown in Table 5.

We see from Table 5, the transition temperature (T_c) of all the composites increases with increase in the concentration of Nb and Sm in BTL and the reason behind this increase may be due to the substitution of Nb and Sm with few Ti ions in BTL composites, as a result the exchange interaction among magnetic Fe^{3+} ions is responsible for the presence of ferromagnetism and this exchange interaction is established through the neighboring octahedrons. Each Fe^{3+}

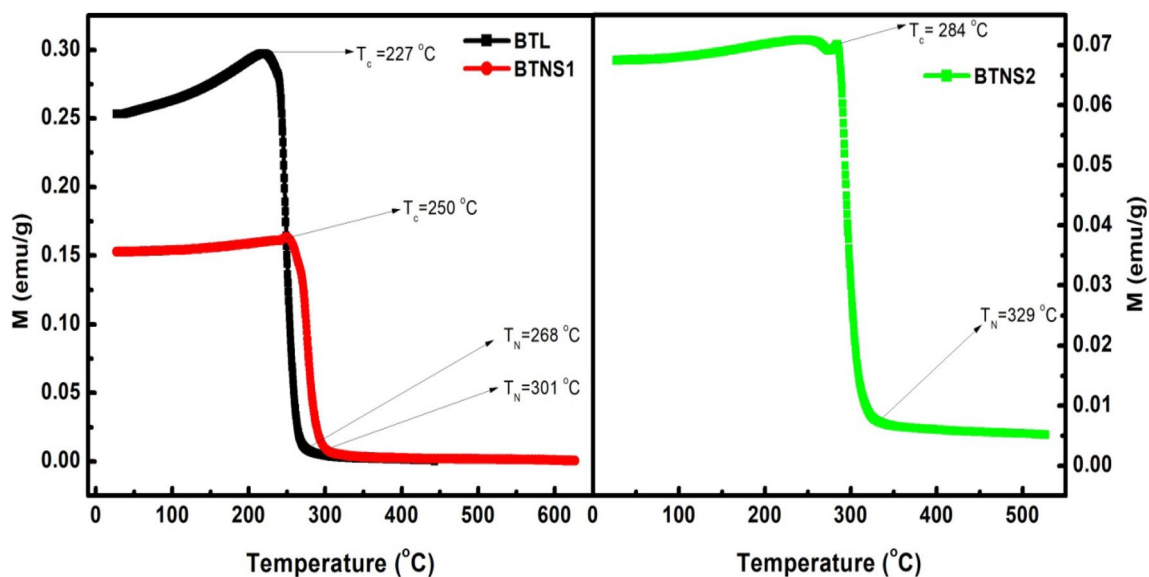
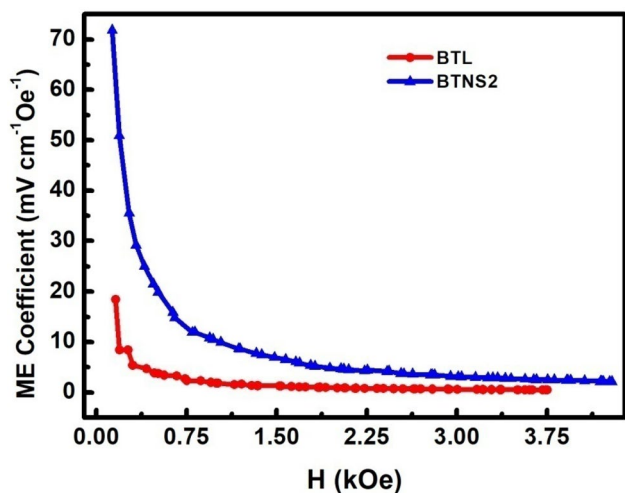


Fig. 8 Magnetization of the BTL, BTNS1 and BTNS2 composite ceramics varies with temperature

Table 5 The values of transition temperature (T_c), Neel temperature (T_N) of BTL, BTNS1 and BTNS2 composite ceramics

Sample	Transition temperature (T_c) °C	Neel temperature (T_N) °C
BTL	227	268
BTNS1	250	301
BTNS2	284	329

**Fig. 9** ME voltage coefficient of the BTNS1 and BTNS2 composite ceramics varies with the magnetic field

ion is located at the center of an octahedron. The exchange interaction will be weakened as more Nb^{5+} and Sm^{3+} ions are doped and occupy more octahedron sites [47, 51]. On account of this weakened interaction, the ferromagnetic nature of the BTL composite decreases which is also clearly evident in Figs. 6 and 7. This decrease in the ferromagnetic nature of the BTL composite after doping it with Nb and Sm can be explained using Weiss Brillouin theory of ferromagnetism. According to the Weiss Brillouin theory of ferromagnetism, when the magnetic spins experience the thermal stirring at non-zero temperature, the internal spins could get reversed leading to the reduction in the magnetisation of all the composites which is clearly seen in Fig. 8 [52]. The Neel temperature of composites increases with increase in the concentration of Nb and Sm in the BTL composite.

3.6 Magneto-electric voltage coefficient

Figure 9 depicts the variation of the Magnetolectric (ME) voltage coefficient with magnetic field of BTL, BTNS2 composites. We see from Fig. 9 that the ME voltage coefficient of composites decreases sharply with increase in the magnetic field upto a certain magnetic field, then become

constant with increase in the magnetic field. The applied magnetic field generates strain in ferromagnetic material inducing stress in the ferroelectric material due to movement of domain walls of both materials and hence a magneto-electric voltage is generated [53]. The variation of ME is similar to that obtained by other workers [54–56].

The ME voltage coefficient of the BTL composite increases after doping Nb and Sm in it at all applied magnetic fields. The magnetolectric effect is a result of piezomagnetic strain in the spinel phase, which creates a piezoelectric charge in the ferroelectric phase and hence it would depend upon the variation of piezomagnetic coefficient with the intensity of the magnetic field [56]. In LF spinel ferromagnetic material, the magnetostrictive coefficient reaches maximum associated with magnetization at a certain value of the magnetic field. Since the strain produced in the ferrite phase would produce a constant electric field in the piezoelectric phase, thereby decreasing dE/dH with increase in H . The ME coefficient value depends on interaction between magnetic and ferroelectric domains, resistivity and also on the molar fraction of magnetic and ferroelectric component. The composites that have lower amount of magnetic components create low strain as well as piezoelectricity [57]. The highest value of ME coefficient may be assigned to its uniform grains and shape. These uniform grains induce strong interaction between the ferroelectric and magnetic orders.

4 Conclusions

We have successively synthesized Sm and Nb doped BTL composites using solid state technique. We have investigated the structural, morphological, magnetic, dielectric and ferroelectric properties of all the composites. The structural studies have confirmed the crystalline nature of the composites. The XRD studies confirmed the tetragonal perovskite structure formation of all the ceramic composites. The XRD peaks of BTNS1 and BTNS2 have shifted towards higher diffraction angle and this strongly confirms the incorporation of Nb and Sm in the BTL composite. This effect is also reflected in the changes in grain size of the BTL composite after doping Nb and Sm in BTL. The grain morphology of the BTNS1 and BTNS2 have changed due to the substitution of Nb and Sm in BTL. The presence of Ba, Ti, O, Fe, Nb and Sm in the prepared composites is confirmed from the EDAX studies. The VSM studies confirmed the soft magnetic nature of the composites. The saturation polarisation and remnant polarisation of BTL are high in comparison with all the composites and both the saturation polarisation and the remnant polarisation decrease with the substitution of Nb and Sm in BTL. The magnetic transition temperature (T_c) of the BTL composite has increased with increase in the concentration of Nb and Sm. The dielectric studies have confirmed that

both the dielectric constant and the dielectric loss of the BTL composite have changed after doping Nb and Sm in it. The electric transition temperature (T_c) of BTNS2 is less than BTNS1 and BTL which may be due to the grain size. The ferroelectric studies have shown that the BTL composite softens upon doping Nb and Sm in it. The ME voltage coefficient of the BTL composite has increased with increase in the concentration of Nb and Sm in BTL at all applied magnetic fields. The undoped and doped BTL composites possess both the ferroelectric and magnetic nature simultaneously and hence they are multiferroic materials which may be used in magnetoelectric sensors, magneto capacitive devices, information storage, electrically driven magnetic data storage spintronics, electro-optic devices and recording.

Acknowledgements We would like to thank Dr. P.D Babu for extending VSM (M-H, M-T) measurements at UGC-DAE Consortium for Scientific Research, Mumbai center, R5-shed, BARC, Mumbai—400 085. We would also like to thank Dr. V. Raghavendra Reddy and Dr. Mukul Gupta of UGC-DAE Consortium for Scientific Research, Indore for extending the facilities P-E loops and XRD and their support. We also thank INUP at IITB for extending the facilities FESEM, dielectric measurements.

References

- J.F. Scott, Multiferroic memories. *Nat. Mater.* **6**(4), 256–257 (2007)
- R. Ramesh, Materials science: emerging routes to multiferroics. *Nature* **461**, 1218–1219 (2009)
- C.H. Sim, Z.Z. Pan, J. Wang, Residual stress and magnetic behavior of multiferroic $\text{CoFe}_2\text{O}_4/\text{Pb}(\text{Zr}_{0.52}\text{Ti}_{0.48})\text{O}_3$ thin films. *J. Appl. Phys.* **105**, 084113–084113 (2009)
- C.W. Nan, Magnetolectric effect in composite of piezoelectric and piezomagnetic phases. *Phy. Rev. B* **50**, 6082–6088 (1994)
- L. Mitoseriu, V. Buscaglia, M. Viviani, M.T. Buscaglia, I. Pallecchi, C. Harnagea, A. Testino, V. Trefiletti, P. Nanni, A.S. Siri, $\text{BaTiO}_3\text{-(Ni}_{0.5}\text{Zn}_{0.5})\text{Fe}_2\text{O}_4$ ceramic composites with ferroelectric and magnetic properties. *J. Eur. Ceram. Soc.* **27**(13–15), 4379–4382 (2007)
- R. Grigalaitisa, M.M. Vijatović Petrovi, J.D. Bobić, A. Dzunuzovic, R. Sobiestianskasa, A. Brilingasa, B.D. Stojanović, J. Banysa, Dielectric and magnetic properties of $\text{BaTiO}_3\text{-NiFe}_2\text{O}_4$ multiferroic composites. *Ceram. Int.* **40**, 6165–6170 (2014)
- Y. Tsur, D.T. Dunbar, A.C. Randall, Crystal and defect chemistry of rare earth cations in BaTiO_3 . *J. Electroceram.* **7**, 25–34 (2001)
- D. Kaur, S. Bindra Narang, K.S. Thind, Processing, dielectric behavior and conductivity of some complex tungsten-bronze dielectric ceramics. *J. Ceram. Process. Res.* **7**(1), 31–36 (2005)
- O.P. Thakur, C. Parkash, D.K. Aggarwal, Structural and electrical properties of microwave-processed BaTiO_3 ceramics. *J. Ceram. Process. Res.* **3**(2), 75–79 (2002)
- M. Aparna, T. Bhimasankaram, S.V. Suryanarayana, G. Prasad, G.S. Kumar, Effect of lanthanum doping on electrical and electromechanical properties of $\text{Ba}_{1-x}\text{La}_x\text{TiO}_3$. *Bull. Mater. Sci.* **24**, 497–504 (2001)
- W. Cai, C. Fu, J. Gao, X. Deng, G. Chen, Z. Lin, Effect of samarium on the microstructure, dielectric and ferroelectric properties of barium titanate ceramics. *Integr. Ferroelectr.* **140**, 92–103 (2012)
- W. Cai, C.L. Fu, J.C. Gao, H.Q. Chen, Effects of grain size on domain structure and ferroelectric properties of barium zirconate titanate ceramics. *J. Alloy. Compd.* **480**(2), 870–873 (2009)
- M.R. Panigrahi, S. Panigrahi, Synthesis and microstructure of Ca-doped BaTiO_3 ceramics prepared by high-energy ball-milling. *Phys. B.* **404**(21), 4267–4272 (2009)
- J. Li, D.R. Jin, L.X. Zhou, Dielectric properties of barium strontium titanate (BST) ceramics synthesized by using mixed-phase powders calcined at varied temperatures. *Mater. Lett.* **76**, 100–102 (2012)
- H.L. Chen, B. Cui, J. Tian, Mn-doped barium titanate nanocrystalline powders and ceramics prepared by sol-gel method. *J. Inorg. Chem.* **23**(8), 1496–1500 (2009)
- S. Anwar, P.R. Sagdeo, N.P. Lalla, Study of the relaxor behaviour in $\text{BaTi}_{1-x}\text{HfxO}_3$ ($0.20 \leq x \leq 0.30$) ceramics. *Solid. State. Sci.* **9**(11), 1054–1060 (2007)
- V.V. Mitic, Z.S. Nikolic, V.B. Pavlovic, Influence of rare-earth dopants on barium titanate ceramics micro structure and corresponding electrical properties. *J. Am. Ceram. Soc.* **93**(1), 132–137 (2010)
- M.C. Ferrarelli, C.C. Tan, D.C. Sinclair, Ferroelectric, electrical, and structural properties of Dy and Sc co-doped BaTiO_3 . *J. Mater. Chem.* **21**(17), 6292–6299 (2011)
- A.K. Nath, N. Medhi, Piezoelectric properties of environmental friendly bismuth doped barium titanate ceramics. *Mater. Lett.* **73**, 75–77 (2012)
- W. Cai, C.L. Fu, J.C. Gao, Dielectric properties and microstructure of Mg doped barium titanate ceramics. *Adv. Appl. Ceram.* **110**(3), 181–185 (2011)
- M.M. Vijatovic Petrovi, C.J.D. Bobi, T. Ramoska, Antimony doping effect on barium titanate structure and electrical properties. *Ceram. Int.* **37**(7), 2669–2677 (2011)
- M. Cernea, C. Galassi, B.S. Vasile, Electrical investigations of holmium-doped BaTiO_3 derived from sol-gel combustion. *J. Mater. Res.* **25**(6), 1057–1063 (2010)
- Y. Yuan, S.R. Zhang, X.H. Zhou, B. Tang, Effects of Nb_2O_5 doping on the microstructure and the dielectric temperature characteristics of barium titanate. *J. Mater. Sci.* **44**(14), 3751–3757 (2009)
- N.A. Rejab, S. Sreekantan, K.A. Razak, Structural characteristics and dielectric properties of neodymium doped barium titanate. *J. Mater. Sci. Mater. Electron.* **22**(2), 167–173 (2011)
- Y.X. Li, X. Yao, X.S. Wang, Studies of dielectric properties of rare earth (Dy, Tb, Eu) doped barium titanate sintered in pure nitrogen. *Ceram. Int.* **38**(S1), S29–S32 (2011)
- T.D. Dunbar, W.L. Warren, B.A. Tuttle, C.A. Randall, Y. Tsur, Electron paramagnetic resonance investigations of lanthanide-doped barium titanate: dopant site occupancy. *J. Phys. Chem. B* **108**, 908–917 (2004)
- P. Om, D. Kumar, R.K. Dwivedi, K.K. Srivastava, P. Singh, S. Singh, Effect of simultaneous substitution of La and Mn on dielectric behavior of barium titanate ceramic. *J. Mater. Sci.* **42**, 5490–5496 (2007)
- D.Y. Lu, M. Toda, M. Sugano, High-permittivity double rare-earth-doped barium titanate ceramics with diffuse phase transition. *J. Am. Ceram. Soc.* **89**(10), 3112–3123 (2006)
- R.F. Zhang, C.Y. Deng, L. Ren, Z. Li, J.P. Zhou, Dielectric, ferromagnetic and magnetolectric properties of $\text{BaTiO}_3\text{-Ni}_{0.7}\text{Zn}_{0.3}\text{Fe}_2\text{O}_4$ composite ceramics. *Mater. Res. Bull.* **48**, 4100–4104 (2013)
- R.S. Devan, S.A. Lokare, D.R. Patil, S.S. Chougule, Y.D. Kolekar, B.K. Chougule, Electrical conduction and magnetolectric effect of $(x) \text{BaTiO}_3 + (1-x) \text{Ni}_{0.92}\text{Co}_{0.03}\text{Cu}_{0.05}\text{Fe}_2\text{O}_4$ composites in ferroelectric rich region. *J. Phys. Chem. Solids* **67**(7), 1524–1530 (2006)

31. J. Zhanga, L. Wanga, L. Biana, J. Xu, A. Chang, Structural, dielectric and piezoelectric properties of $x\text{BiFeO}_3-(1-x)\text{BaTi}_{0.9}\text{Zr}_{0.1}\text{O}_3$ ceramics. *Ceram. Int.* **40**(4), 5173–5179 (2014)
32. B.D. Stojanovic, C.R. Foschini, M.A. Zaghete, F.O.S. Veira, K.A. Peron, M. Cilense, J.A. Varela, Size effect on structure and dielectric properties of Nb-doped barium titanate. *J. Mater. Proc. Technol.* **802**, 143–144 (2003)
33. S.K. Upadhyaya, V. Raghavendra Reddy, N. Lakshmi, Study of $(1-x)\text{BaTiO}_3-x\text{Ni}_{0.5}\text{Zn}_{0.5}\text{Fe}_2\text{O}_4$ ($x=5, 10$ and 15%) magneto-electric ceramic composites. *J. Asian Ceram. Soc.* **1**, 346–350 (2013)
34. W. Cai, S. Zhong, C. Fu, G. Chen, X. Deng, Microstructure, dielectric and ferroelectric properties of $x\text{BaZr}_{0.2}\text{Ti}_{0.8}\text{O}_3-(1-x)\text{BiFeO}_3$ solid solution ceramics. *Mater. Res. Bull.* **50**, 259–267 (2014)
35. T. Dechakupt, J. Tangsritrakul, P. Ketsuwan, R. Yimnirun, Microstructure and electrical properties of niobium doped barium titanate ceramics. *Ferroelectrics* **415**, 141–148 (2011)
36. W. Cao, C.A. Randall, Grain size and domain size relations in bulk ceramic ferroelectric materials. *J. Phys. Chem. Solids* **57**, 1499–1505 (1996)
37. Z. Yu, C. Ang, Maxwell–Wagner polarization in ceramic composites $\text{BaTiO}_3-(\text{Ni}_{0.3}\text{Zn}_{0.7})\text{Fe}_{2.1}\text{O}_4$. *J. Appl. Phys.* **91**, 794–797 (2002)
38. Y.J. Li, X.M. Chen, R.Z. Hou, Y.H. Tang, Maxwell–Wagner characterization of dielectric relaxation in $\text{Ni}_{0.8}\text{Zn}_{0.2}\text{Fe}_2\text{O}_4/\text{Sr}_{0.5}\text{Ba}_{0.5}\text{Nb}_2\text{O}_6$ composite. *Solid State Commun.* **137**, 120–125 (2006)
39. Y.Q. Lin, X.M. Chen, Dielectric relaxations in $\text{Sr}_{0.5}\text{Ba}_{0.5}\text{Nb}_2\text{O}_6/\text{CoFe}_2\text{O}_4$ high- ϵ magnetolectric composite ceramics. *Mater. Chem. Phys.* **117**, 125–130 (2009)
40. Y. Wang, Y. Wang, W. Rao, M. Wang, G. Li, Y. Li, J. Gao, W. Zhou, J. Yu, Dielectric, ferromagnetic and ferroelectric properties of the $(1-x)\text{Ba}_{0.8}\text{Sr}_{0.2}\text{TiO}_3-x\text{CoFe}_2\text{O}_4$ multiferroic particulate ceramic composites. *J. Mater. Sci. Mater. Electron.* **23**, 1064–1071 (2012)
41. P. Richa Sharma, R.P. Pahuja, Tandon, Structural, dielectric, ferromagnetic, ferroelectric and ac conductivity studies of the $\text{BaTiO}_3-\text{CoFe}_{1.8}\text{Zn}_{0.2}\text{O}_4$ multiferroic particulate composites. *Ceram. Int.* **40**, 9027–9036 (2014)
42. A. Gupta, R. Chatterjee, Dielectric and magnetolectric properties of $\text{BaTiO}_3-\text{Co}_{0.6}\text{Zn}_{0.4}\text{Fe}_{1.7}\text{Mn}_{0.3}\text{O}_4$ composite. *J. Eur. Ceram. Soc.* **33**, 1017–1022 (2013)
43. M.J. Miah, M.N.I. Khan, A.K.M.A. Hossain, Weak ferromagnetism and magnetolectric effect in multiferroic $x\text{Ba}_{0.95}\text{Sr}_{0.05}\text{TiO}_3-(1-x)\text{BiFe}_{0.9}\text{Gd}_{0.1}\text{O}_3$ relaxors. *J. Magn. Mater.* **401**, 600–611 (2016)
44. X. Wang, X. Xu, W. Gong, Z. Feng, R. Gong, Electromagnetic properties of Fe-Si-Al/BaTiO₃/Nd₂Fe₁₄B particulate composites at microwave frequencies. *J. Appl. Phys.* **115**, 17C722 (2014)
45. A.A. Sattar, S.A. Rahman, Dielectric properties of rare earth substituted Cu–Zn ferrites. *Phys. Status Solidi A* **200**(2), 415–422 (2003)
46. B. Y. Wang, H.T. Wang, S.B. Singh, Y.C. Shao, Y.F. Wang, C.H. Chuang, P.H. Yeh, J.W. Chiou, C.W. Pao, H.M. Tsai, H.J. Lin, J.F. Lee, C.Y. Tsai, W.F. Hsieh, M.-H. Tsai, W.F. Pong, *RSC Adv.* **3**, 7884–7893 (2013)
47. C. Lan, Y. Jiang, S. Yang, Magnetic properties of La and (La, Zr) doped BiFeO₃ ceramics. *J. Mater. Sci.* **46**, 734–738 (2011)
48. A. Srinivas, R. Gopalan, V. Chandrasekharan, Room temperature multiferroism and magnetolectric coupling in BaTiO₃–BaFe₁₂O₁₉ system. *Solid State Commun.* **149**, 367 (2009)
49. R.C. Kambale, N.R. Adhate, B.C. Chougule, Y.D. Kplekar, Magnetic and dielectric properties of mixed spinel Ni–Zn ferrites synthesized by citrate–nitrate combustion method. *J. Alloys Compd.* **491**, 372–377 (2010)
50. R.S. Devan, B.K. Chougule, Effect of composition on coupled electric, magnetic and dielectric properties of two phase particulate magnetolectric composite. *J. Appl. Phys.* **101**, 014109–014114 (2007)
51. G.P. Du, Z.J. Hu, Q.F. Han, X.M. Qin, W.Z. Shi, Effects of niobium donor doping on the phase structures and magnetic properties of Fe-doped BaTiO₃ ceramics. *J. Alloy. Compd.* **492**, L79–L81 (2010)
52. A. Singh, V. Pandey, R.K. Kotnala, D. Pandey, Direct evidence for multiferroic magnetolectric coupling in 0.9BiFeO₃–0.1BaTiO₃. *Phys. Rev. Lett.* **101**, 247602–247601 (2008)
53. P. Pahuja, R.K. Kotnala, R.P. Tandon, Effect of rare earth substitution on properties of barium strontium titanate ceramic and its multiferroic composite with nickel cobalt ferrite. *J. Alloy. Compd.* **617**, 140–148 (2014)
54. K.K. Patankar, P.D. Dombale, V.L. Mathe, S.A. Patil, R.N. Patil, AC conductivity and magnetolectric effect in MnFe_{1.8}Cr_{0.2}O₄–BaTiO₃ composites. *Mater. Sci. Eng. B* **87**, 53–58 (2001)
55. T.G. Lupieko, I.B. Lopatina, I.V. Kozyrev, L.A. Derbaremdiker, Electrophysical and magnetolectric properties of ceramic materials of the type piezoelectric-ferrite. *Inorg. Mater.* **28**, 481–485 (1992)
56. J. Van den Boomgaard, R.A.J. Born, A sintered magnetolectric composite material BaTiO₃–Ni(Co, Mn)Fe₂O₄. *J. Mater. Sci.* **13**, 1538–1548 (1978)
57. C.W. Nan, Magneto-electric effect in composites of piezoelectric and piezo magnetic phases. *Phys. Rev. B* **50**, 6082–6088 (1994)